Prediction of Electropolymerization Mechanisms of Two Substituted Phenylene: Poly-3-methoxy-toluenes ($P3mt_1$ and $P3mt_2$)

S. Ayachi,[1] S. Bouzakraoui,[2] M. Hamidi,[2] M. Bouachrine,[2] P. Molinié,[3] K. Alimi[1]

[1]*Unité de Recherche, Matériaux Nouveaux et Dispositifs Electroniques Organiques, Faculté des Sciences de Monastir, 5000 Monastir, Tunisie*
[2]*LRMM, Faculté des Sciences et Techniques, B.P. 509, Boutalamine, Errachidia, Maroc*
[3]*Institut des Matériaux Jean Rouxel, CNRS-UMR 6502, 2, rue de la Houssinière, BP 32229, 44322 Nantes cedex 3, France*

Received 19 April 2005; accepted 15 July 2005
DOI 10.1002/app.22640
Published online 4 January 2006 in Wiley InterScience (www.interscience.wiley.com).

ABSTRACT: $P3mt_1$ and $P3mt_2$ were electrochemically synthesized using two different electrolyte supports H_2SO_4 and $TEABF_4$, respectively. First, it was deduced from density functional theory (DFT) calculations that the electronic and steric effects govern polymerization mechanism of the radical monomers. Second, DFT combined with experimental spectroscopic analyses (ESR, Infrared, Raman, and ^{13}C NMR) demonstrate that H_2SO_4 or $TEABF_4$ could generate a homogenous or heterogeneous coupling site, respectively. © 2006 Wiley Periodicals, Inc. J Appl Polym Sci 100: 57–64, 2006

Key words: ESR; DFT; radical polymerization; spin density; structure–property relations.

INTRODUCTION

Even without X-ray spectra, the structure–properties relationships of organic polymers remain well understood. Although density functional theory (DFT) calculations are employed only for a limited number of monomers,[1,2] it can help for a better description of the polymer structure.[3–7] To explore polymers with precisely defined molecular architecture in specific optoelectronic applications, polymer physicists would like to work with well-defined polymeric materials having structural homogeneity.[8] Such model materials provide the opportunity to better explore structure–properties relationships. However, the polymer physicists appreciate the role of the polymer chemists and do not underestimate their significant contribution to the field of polymer physics. To interpret the optical results of polymers, the physicists are obliged to start with a structure that can be not optimal. In this work, we are going to combine the DFT calculations with experimental results on two types of poly-3-methoxy-toluenes (P3mt). The two materials denoted as $P3mt_1$ and $P3mt_2$ are electrochemically synthesized using two electrolyte supports H_2SO_4 and $TEABF_4$, respectively.[9] Theoretical results are combined with the experimental ones to describe the electropolymerization mechanisms of both polymers. In this study, the unpaired electron spin densities of radical cations, which allow the knowledge of the reactivity for coupling reactions,[1] are calculated for oligo-3mt (from dimers to seximers) using DFT of three-parameter compound functional of Becke (B3LYP). The 6–31G(d) basis set was used for all calculations. The geometric structures of neutral molecules were optimized under no constraints. Ionization potentials were computed as the energy differences between a neutral molecule and the respective radical cations. Furthermore, geometry structures of radical cations were optimized independently from the neutral molecules prior to the calculations of spin densities. Radical cations were treated as open shell systems (B3LYP). All calculations were performed using the Gaussian 98 program.[10]

EXPERIMENTAL

Electron spin resonance (ESR) experiments were performed at room temperature on a Bruker ER 200 D spectrometer operating at X band. The interpretation of the ESR spectrum was made using the pole method,[11] with a Gaussian or a Lorentzian or a mixture of the two line shapes described elsewhere.[12,13] The comparison between experimental and theoretical spectrum yields the parameters of each Zeeman distribution.

Infrared and Raman spectra were measured at room temperature using a Brucker Vector 22 spectropho-

Correspondence to: K. Alimi (kamel.alimi@fsm.rnu.tn).

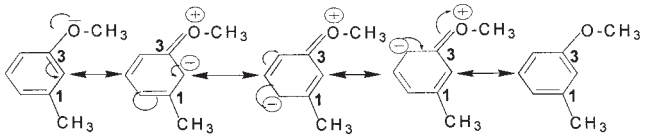

Figure 1 Resonance structures of 3mt monomer.

tometer and spectrometer Bruker RFS 100, using a laser wavelength 1060 nm, respectively. Band positions are expressed in wavenumbers (cm^{-1}) from 400 to 1750. For infrared measurements, the samples were pellets of KBr mixed with the organic compound under study.

NMR spectra were acquired at room temperature using a Bruker Advance 500 MHz spectrometer operating at 125.7 MHz for ^{13}C, using a 4-mm double-bearing Bruker probehead. Spectra were referenced to TMS for ^{13}C, using adamantane as a secondary reference.{^{1}H}-^{13}C CPMAS (cross-polarization magic-angle-spinning) NMR spectra were acquired using a ramp-amplitude sequence,[14] a 2 ms contact time and a repetition time of 2 s. ^{1}H decoupling during acquisition was achieved using the TPPM method[15] with a RF field of ~60 kHz. MAS spinning rates were set between 10 and 15 kHz.

Use of DFT calculations to predict monomer-coupling sites

Analogues with pyrrole[16] and thiophene[17] polymerization process, the 3-methoxy-toluene (3mt) electrpolymerization starts with one-electron oxidation of the monomer to form its radical cation. The electronic distribution of the radical cation is explained by the resonance structures represented in Figure 1. DFT calculated total atomic spin densities of this radical cation (**1*a***) are shown in Figure 2.

For the optimized 3mt radical cation (**1*a***), DFT calculations revealed that the highest significant spin

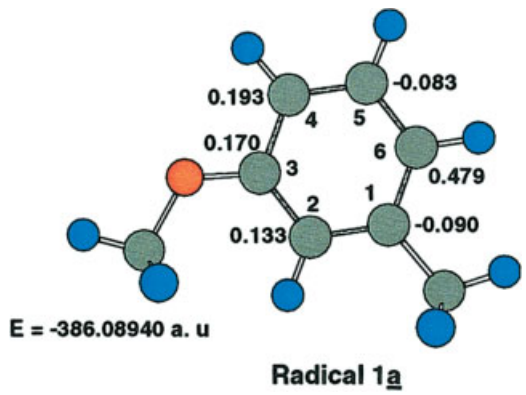

Figure 2 Spin density populations of the optimized radical cation **1*a***.

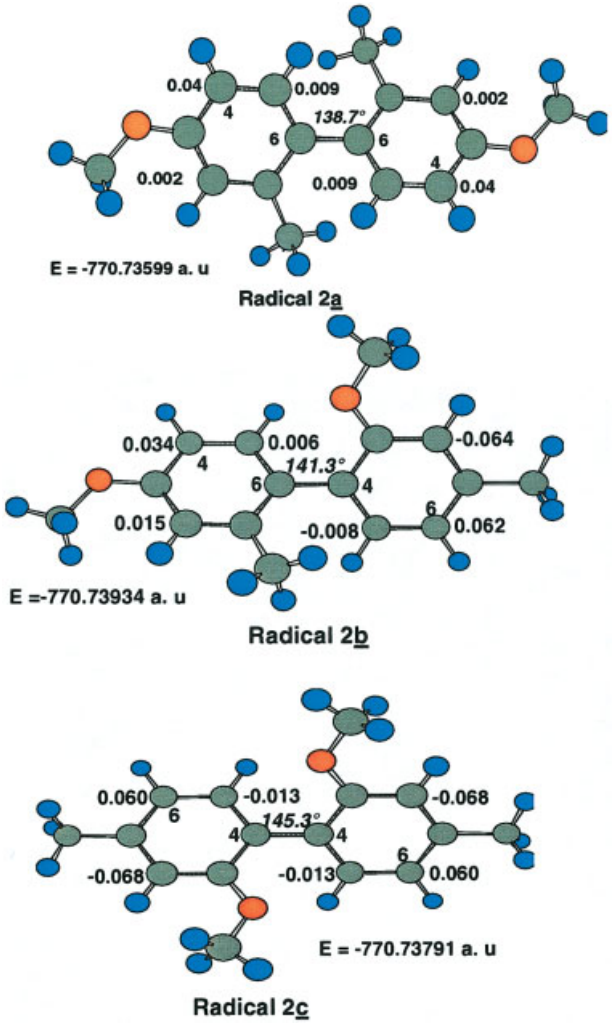

Figure 3 Spin density populations and dihedral angles of the three dimers: **3*a***, **3*b***, and **3*c***. [Color figure can be viewed in the online issue, which is available at www.interscience.wiley.com.]

density (0.48) is located on 6-carbon (C_6) and also a relatively high spin density (0.19) is observed on 4-carbon (C_4). However, lower spin densities (0.01 and −0.08) are calculated for the carbons 2 and 5, respectively. We deduce that the coupling between two radical cations to form the dimers will take place preferentially between the 6- and 4-carbon sites. The spin density at C_6 is much higher than that at C_4, indicating that the C_6 is much more reactive than the C_4.

The dimerization of 3mt monomers consists of two-step reactions: oxidation and deprotonation of the dimer. However, when two molecules of 3mt monomer are chemically coupled, coupling occurs primarily through the 6- and 4-carbon atoms of the phenyl ring. These positions exhibit the highest unpaired electron π-spin density and they are, hence, the most reactive. Accordingly, three most probable couplings 6−6 (**2*a***), 6−4 (**2*b***), and 4−4 (**2*c***) can be generated (Fig. 3) neighboring other minority dimers generated via

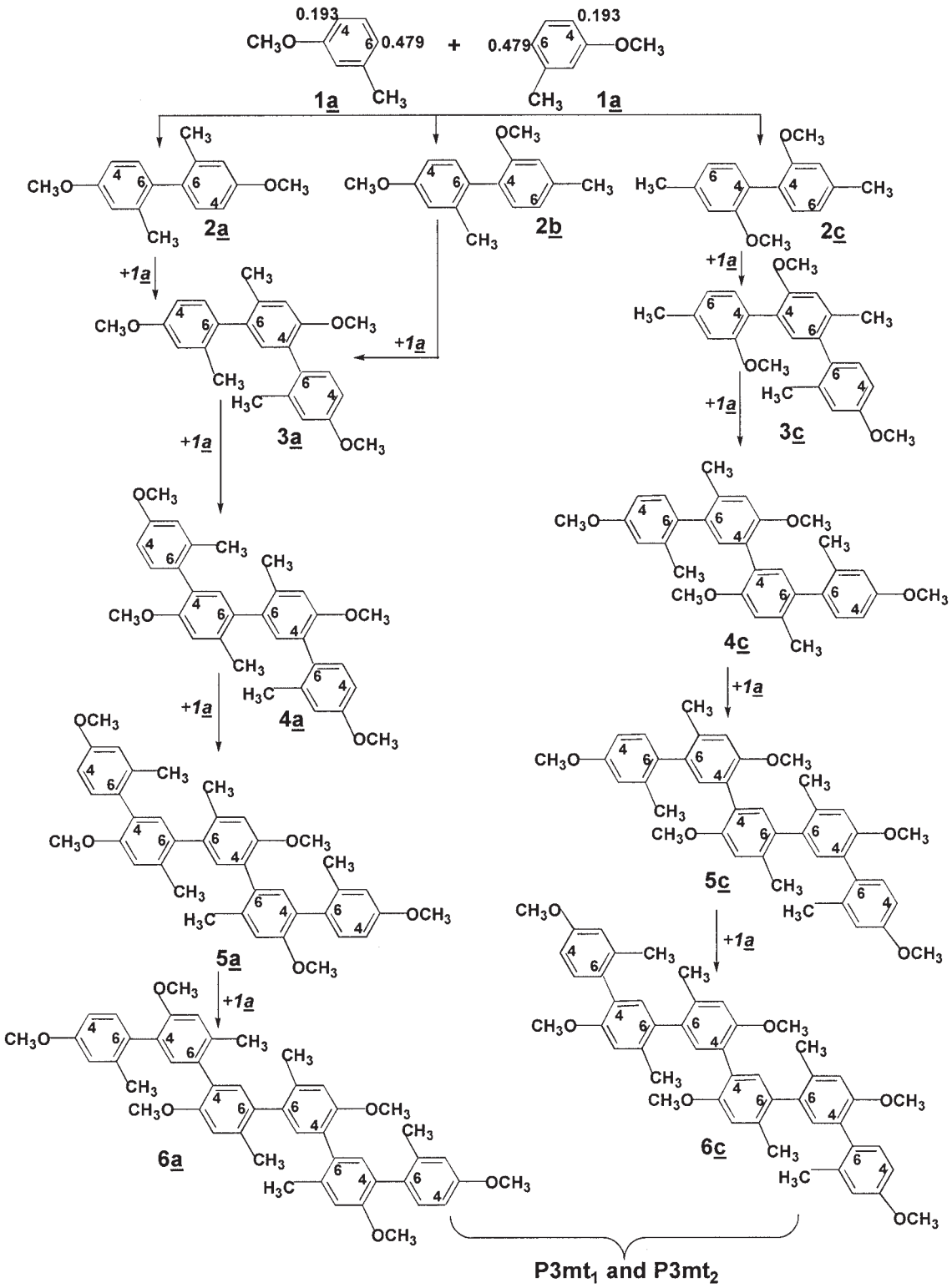

Figure 4 Reaction paths of the succeeding coupling reactions of 3mt radical based on spin densities calculation.

couplings with 2-carbon site. It's worth mentioning that less steric hindrance is observed in the dimer **2*a***, which presents CH_3/CH_3 junction (dihedral angle φ_{2a} = 138.7°) compared with the other cases (φ_{2b} = 141.3° and φ_{2c} = 145.3°). Added to this, the **2*a*** product is less stable (more reactive) than **2*b*** and **2*c*** ($\Delta E = E_{2a} - E_{2b}$ = 2.1 kcal mol^{-1}and $\Delta E = E_{2a} - E_{2c}$ = 1.0 kcal mol^{-1}).

The ionization potential values deduced from DFT calculations in the case of the monomer **1*a*** is 7.6 eV and for the dimer **2*a*** is 6.7 eV. It was demonstrated

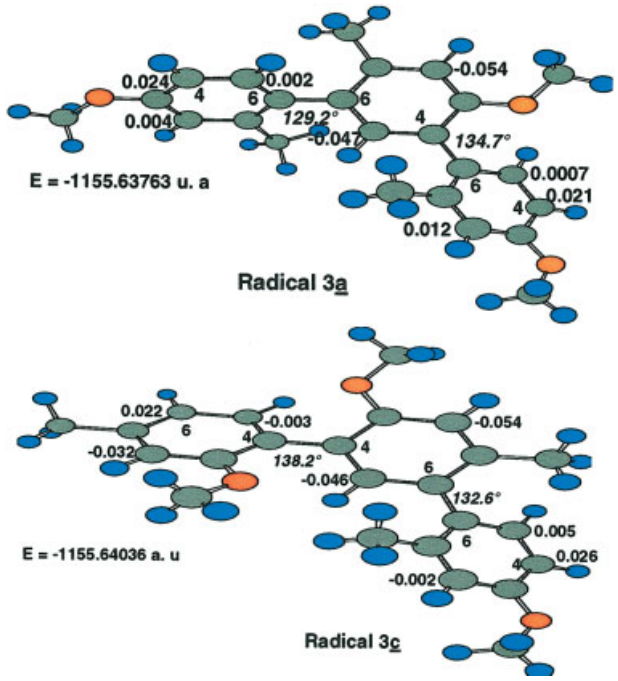

Figure 5 Spin density populations and dihedral angles of the two trimers: **3*a*** and **3*c***. [Color figure can be viewed in the online issue, which is available at www.interscience.wiley.com.]

that small amounts of sulfuric acid is found to favor the electro-oxidation of benzene by lowering the oxidation potential of the monomer.[18] As a result of easy

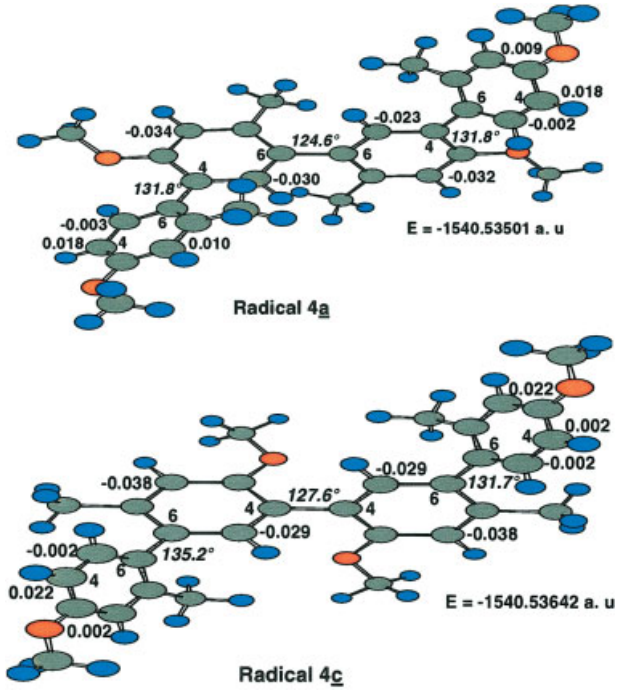

Figure 6 Spin density populations and dihedral angles of the two tetramers: **4*a*** and **4*c***. [Color figure can be viewed in the online issue, which is available at www.interscience.wiley.com.]

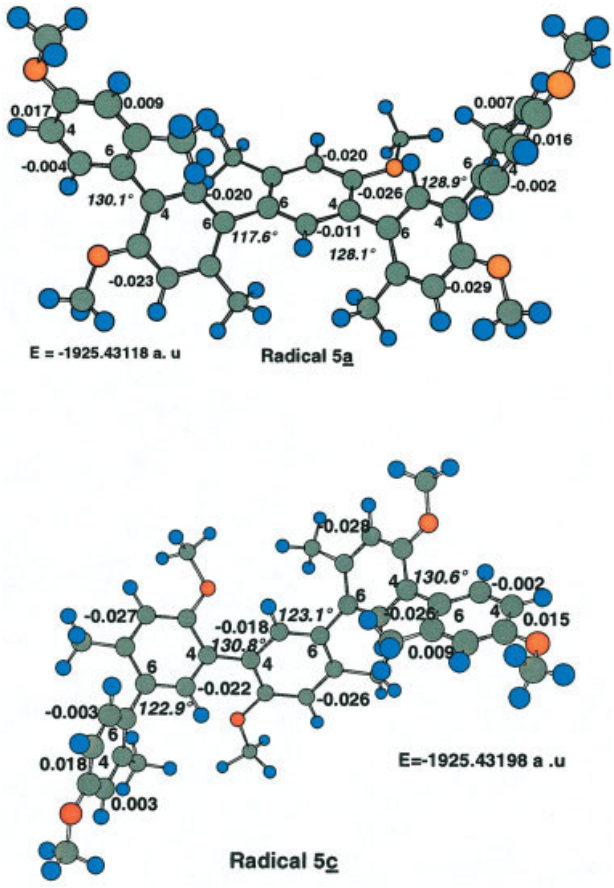

Figure 7 Spin density populations and dihedral angles of the two pentamers: **5*a*** and **5*c***. [Color figure can be viewed in the online issue, which is available at www.interscience.wiley.com.]

oxidation of the dimer than the monomer, the progression mechanism continues via the same sequence: oxidation, coupling, and deprotonation until the final polymer is obtained.

According to the initial propagating reactions, we deduce that coupling reactions preferentially occur between the carbons having higher spin density.[19] In Figure 4, we present a schematic reactions path of the oligomerization mechanism of 3mt.

The coupling between radical cation **2*a*** or **2*b*** and **1*a*** produce the **3*a***-trimer, while the coupling of radical **2*c*** with **1*a*** leads to the radical **3*c*** formation (Fig. 4). The radical **3*a*** has two dihedral angles equal to 129.2° and 134.7° compared with those of radical **3*c*** (138.2° and 132.6°) (Fig. 5). The calculated energy difference of both trimers is evaluated to be about 1.7 kcal mol^{-1}. Thus, the trimer **3*a*** appears more reactive than **3*c***.

The polymerization mechanisms continue in the same reactivity protocol based on the spin density at the terminus carbon sites of each oligomer (**4*a***, **4*c***, **5*a***, and **5*c***) (Figs. 6 and 7). The most probable hexamers are **6*a*** and **6*c*** and their optimization geometries are presented in Figure 8.

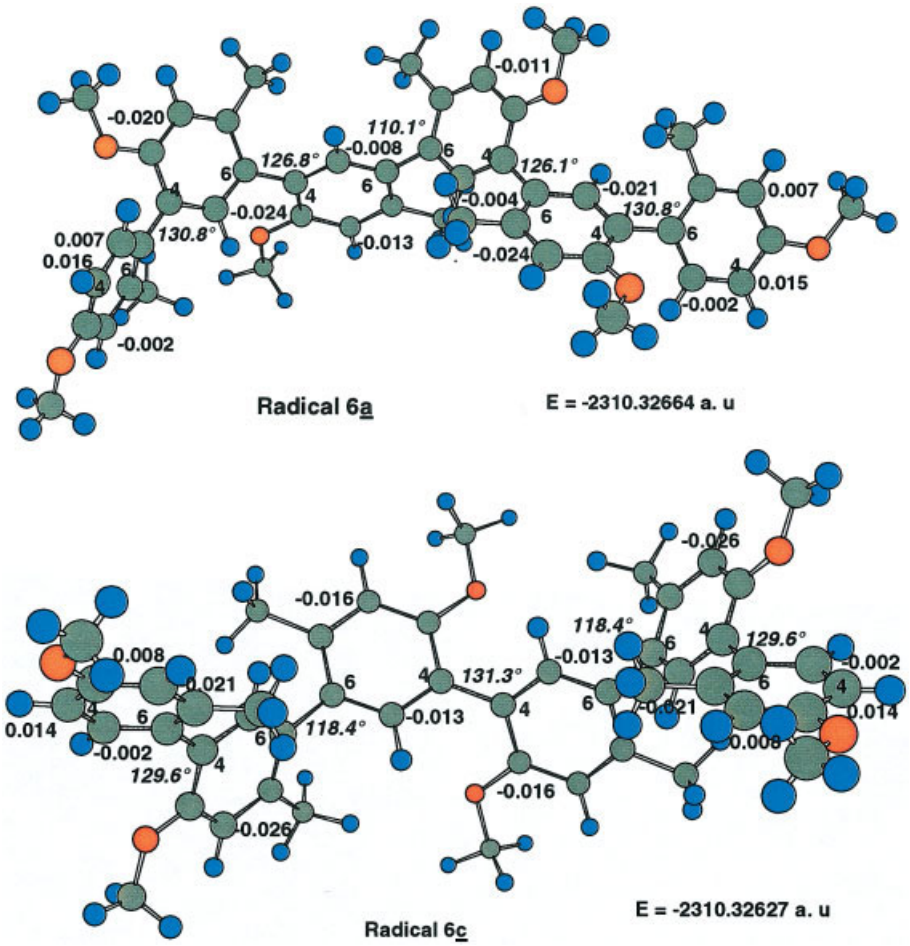

Figure 8 Spin density populations and dihedral angles of the two seximers: **6*a*** and **6*c***. [Color figure can be viewed in the online issue, which is available at www.interscience.wiley.com.]

At this stage and concerning the calculated spin density of each oligomer, we argue our assumption that the most probable path of propagation is thus **1*a*→2*a*→3*a*→4*a*→5*a*→6*a***. The obtained results of the optimized oligo-3mt structures prove that increasing number of 3mt units lead to a decrease of the electron π-spin density particularly at the C_6 or C_4 terminus site positions. Let us note that oligomer is addressed as prototype model of polymers,[3] and it is useless to run calculations for higher oligomers.

DISCUSSION

To justify the electropolymerization mechanisms of P3mt polymers, we recall some spectroscopic analyses, such as ESR, infrared and Raman, and nuclear magnetic resonance (^{13}C NMR).

Recently, electrolyte effect on the polymer properties has been studied mainly by ESR.[20] In this system, paramagnetic radical centers are generated upon electropolymerization process. At room temperature, for both P3mt polymers a well-resolved ESR signal was observed. The deconvolution of their ESR spectra showed that for the P3mt$_1$, only one isotropic Lorentzian Zeeman distribution $D_{1,1}(g_{1,1}\ (xyz) = 2.0022$ and wd = 0.45 mT) [Fig. 9(a)] is observed. However, in the case of P3mt$_2$, two anisotropic Lorentzian Zeeman distributions {$D_{2,\,1}$ ($g_{2,1}$ (xy) = 2.0025, $g_{2,1}$ (z) = 1.9995, wd = 0.42_5 mT) and $D_{2,2}$ ($g_{2,2}$ (xy) = 2.0053, $g_{2,2}$ (z) = 1.9987, wd = 0.40 mT} and an isotropic Lorentzian Zeeman distribution {$D_{2,3}$ ($g_{2,3}$ (xyz) = 1.9985, wd = 0.30 mT} are observed [Fig. 9(b)].

It can be seen from Raman spectra [Fig. 10(a,b)] that a well-resolved band absorption located at 723 cm^{-1} is observed in the case of P3mt$_2$ unlike for P3mt$_1$. This peak is attributed to the meta-substituted phenylene rings.[21] However, the presence of meta-substituted phenylene peak is confirmed by infrared analyses for two P3mt polymers (Fig. 11). Then, their absorption band is shown at about 660 cm^{-1}.

For the ^{13}C NMR solid-state spectra of P3mt polymers (Fig. 12), at first, for the sake of comparison, similar evidences were obtained from ^{13}C NMR spectrum of P3mt$_1$ and P3mt$_2$. Consequently, we note that there are no changes in peak positions (chemical shifts). In general, the structural effect on molecular

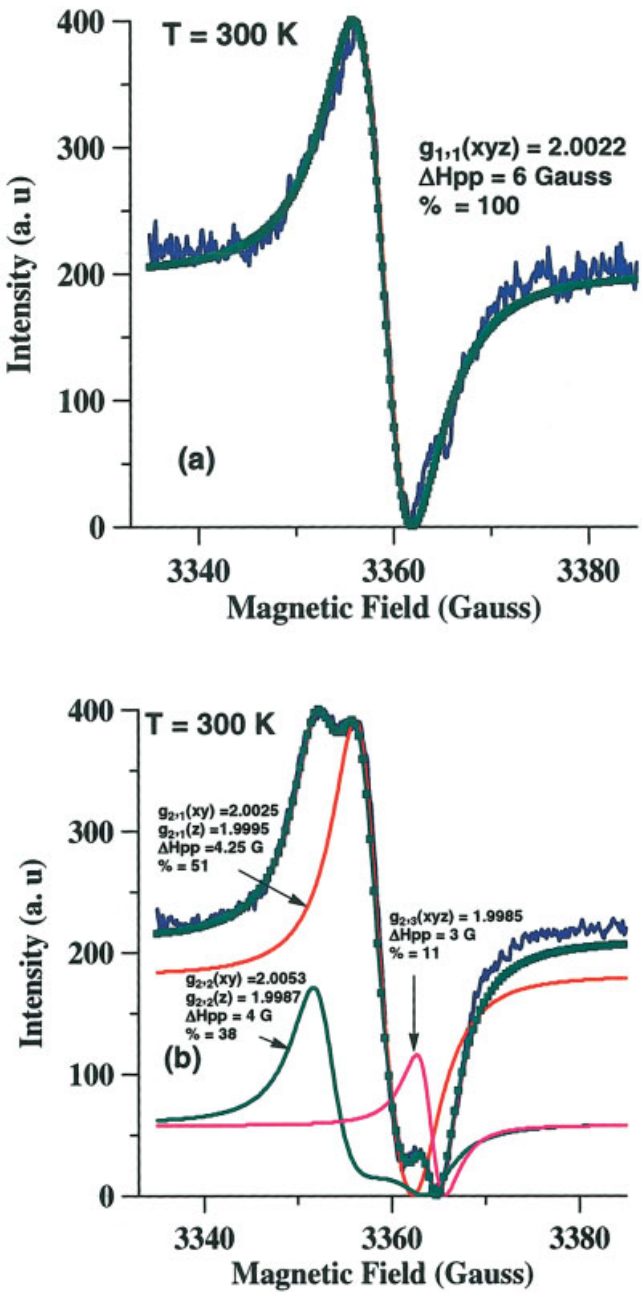

Figure 9 ESR spectra decomposition at room temperature of $P3mt_1$ (a) and $P3mt_2$ (b). [Color figure can be viewed in the online issue, which is available at www.interscience.wiley.com.]

geometry is associated with substituents that due to their inductive and mesomeric interactions effect may cause substantial changes particularly in dihedral angles. In parallel, we check that strong peaks with a smaller chemical shift at 20 and 57 ppm were assigned to carbons in methyl (CH_3) and methoxy (OCH_3) groups, respectively. The other shifts can be assigned to many sorts of aromatic carbons.

The synthetic protocol of $P3mt_1$ and $P3mt_2$, which involves respectively the two electrolyte supports H_2SO_4 and $TEABF_4$, can be explained by the difference of SO_4^{2-} and BF_4^- anions size. In fact, the big size of BF_4^- compared with that of SO_4^{2-} hinders the reaction process, thus generating screen effect on the carbon sites that are able to establish polymerization. Accordingly, in the presence of $TEABF_4$, we assist to a heterogeneous coupling (presence simultaneously of 6–6, 4–4, and 6–4 junctions: CH_3/CH_3, OCH_3/OCH_3, and CH_3/OCH_3).

The appearance of a relatively intense peak of meta-substituted phenylene ring in the infrared spectrum (660 cm^{-1}) of $P3mt_1$ compared with $P3mt_2$ justify well the polymerization reaction leading to an homogenous coupling (junction 6–4:CH_3/OCH_3) and argue the most probable proposed reaction path. ESR results are in good agreement with those of DFT calculations and experimental measurements. These results converge to propose the more organized oligomeric structure when using H_2SO_4 as electrolyte support. In con-

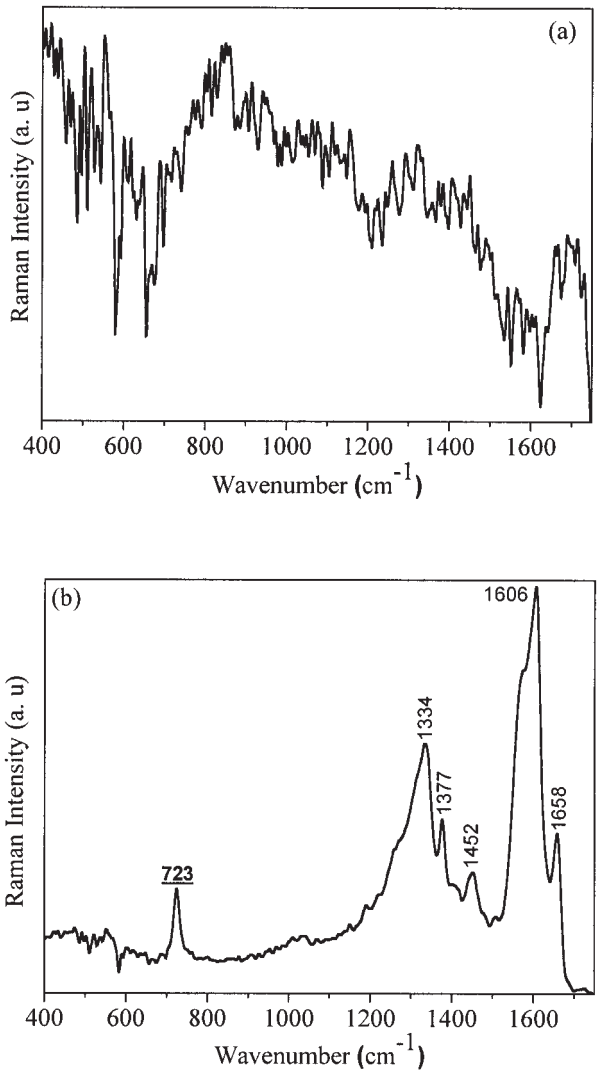

Figure 10 Experimental Raman spectra of P3mt polymers: (a) $P3mt_1$ and (b) $P3mt_2$.

trast, the presence of anisotropic paramagnetic centers explained the heterogeneity of the product when $TEABF_4$ is used.

Furthermore, the most significant difference found in ^{13}C NMR spectra was related to the intensity of the methoxy side chains, unlike for the methyl group. It appears that chemical shift values in ^{13}C NMR spectroscopy depend on the steric and mesomeric effects introduced by methoxy side chains. Moreover, the effect of substituents on ^{13}C NMR chemical shifts is sensitive to π-electron populations. In our opinion, as the methoxy groups (with mesomeric effect +M) have in fact an enhanced steric hindrance compared to methyl groups (with inductive effect +I),[22] based on theoretical electron spin densities and resonance structures for each polymers, we would attribute the unknown chemical shifts assigned to the aromatic carbons. In fact, the observed chemical shifts at 112, 124, 132, 134, and 158 ppm are attributed, respectively, to 2, 5, 1, 4/6, and 3 carbons aromatic rings.

Because of the dipolar interactions occurring in all case of polymers, it seems that ^1H NMR spectroscopy is useless in this investigation. At the same time, it appears that theoretical calculations become very heavy when the number of monomers increases. Consequently, it is difficult to optimize structures with seven monomer units. Furthermore, ESR analysis showed that only one isotropic line is observed in the case of P3mt$_1$, whereas in the case of P3mt$_2$, an ESR isotropic and two other anisotropic lines with percentage values equal to 11, 38, and 51% are, respectively, observed. We think that P3mt$_1$ powder is obtained following the ***6a*** sequences type, where the entire time, paramagnetic radical, is carried with 2-carbon (C_2). In the case of P3mt$_2$ powder, the percentages ESR line values are proportional to 1, 3, and 5, respectively. This indicates the presence of 6, 4, and 2 carbons with number 1, 3, and 5, respectively. Then, P3mt$_2$ is a mixture of 6–6, 4–4, 6–4, and 2–2 bridging types.

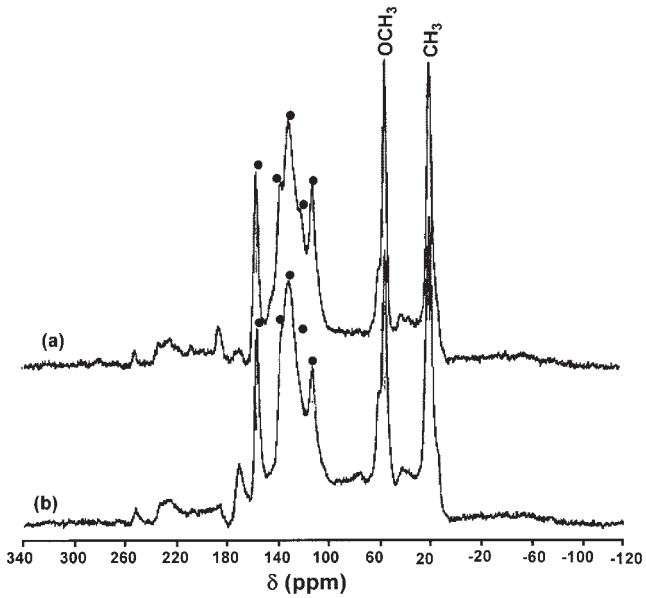

Figure 12 ^{13}C NMR spectra of P3mt polymers: (a) P3mt$_1$ and (b) P3mt$_2$.

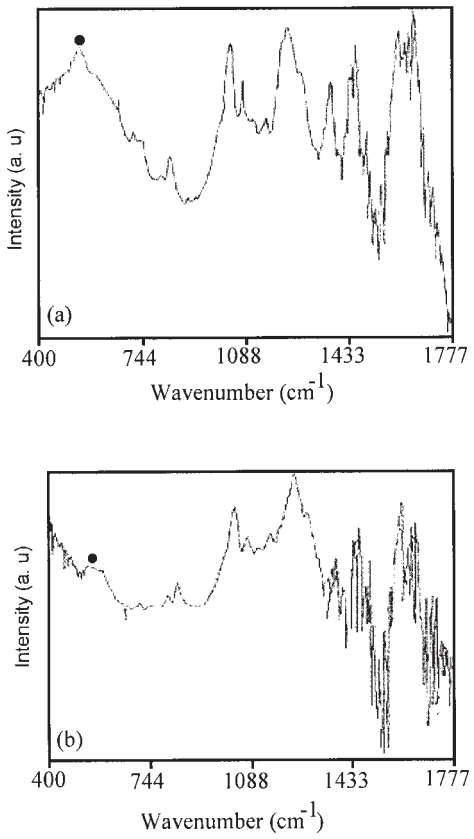

Figure 11 Experimental infrared spectra of P3mt polymers: (a) P3mt$_1$ and (b) P3mt$_2$.

CONCLUSIONS

In this paper, we first checked that with 3mt oligomers, B3LYP/6–31G(d) calculations give reliable results with experimental ones. The electropolymerization mechanism is governed by two factors, the electronic and steric effects. Based on the reactivity of C_4 and C_6 carbons, energy optimization stabilization values, and dihedral angles, we predict the most oligomerization mechanism via the proposed reaction paths of the succeeding coupling reactions of 3mt monomer ***1a***. According to the experimental results, we have predicted the electropolymerization mechanisms of the P3mt polymers. It appears that P3mt$_1$ (H_2SO_4) and P3mt$_2$ ($TEABF_4$) were obtained following the sequence of ***6a*** and a mixture of ***6c***/2–2 coupling sites, respectively.

References

1. Ando, S.; Ueda, M. Synth Met 2002, 129, 207.
2. Honda, K.; Furukawa, Y. Synth Met 2003, 135–136, 335–336.

3. Slazner, U.; Lagowski, J. B.; Pickup, P. G.; Poirier, R. A. Synth Met 1998, 96, 177.
4. Pogantsch, A.; Mahler, A. K.; Hayn, G.; Saf, R.; Stelzer, F.; List, E. J. W.; Brédas, J. L.; Zoger, E. Chem Phys 2004, 297, 143.
5. Seong, S.; Lee, M. E.; Lee, T. B.; No, K. T.; Kim, H. K. Synth Met 2004, 141, 251.
6. Champagne, B.; Mosley, D. H.; Fripiat, J. G.; Andre, J. M. Phys Rev B 1996, 54, 2381.
7. Miao, M. S.; Van Doren, V. E.; Van Camp, P. E.; Straub, G. Comput Mater Sci 1998, 10, 362.
8. Hadjichristidis, N. Eur Phys J E 2003, 10, 83.
9. Bergaoui, S.; Saïd, A. H.; Matoussi, F. Eur Polym Mater 2002, 38, 1731.
10. Frisch, M. J.; Trucks, G. W.; Schlegel, H. B.; Scuseria, G. E.; Robb, M. A.; Cheeseman, J. R.; Zakrzewski, V. G.; Montgomery, J. A. Jr.; Stratmann, R. E.; Burant, J. C.; Dapprich, S.; Millam, J. M.; Daniels, A. D.; Kudin, K. N.; Strain, M. C.; Farkas, O.; Tomasi, J.; Barone, V.; Cossi, M.; Cammi, R.; Mennucci, B.; Pomelli, C.; Adamo, C.; Clifford, S.; Ochterski, J.; Petersson, G. A.; Ayala, P. Y.; Cui, Q.; Morokuma, K.; Malick, D. K.; Rabuck, A. D.; Raghavarchari, K.; Foresman, J. B.; Cioslowski, J.; Ortiz, J. V.; Baboul, A. G.; Stefanov, B. B.; Liu, G.; Liashenko, A.; Piskorz, P.; Komaromi, I.; Gomperts, R.; Martin, R. L.; Fox, D. J.; Keith, T.; Al-Laham, M. A.; Peng, C. Y.; Nanayakkara, A.; Gonzalez, C.; Challacombe, M.; Gill, P. M. W.; Johnson, B.; Cheng, W.; Wong, M. W.; Andres, J. L.; Head-Gordon, M.; Replogle, E. S. and Pople, J. A. Gaussian 98, Revision A.7, Gaussian, Inc.: Pittsburgh, PA, 1998.
11. Angot, A. Complément de mathématiques: Masson, Paris, 1972; p 27.
12. Zaidi, B.; Ayachi, S.; Mabrouk, A.; Molinié, P.; Alimi, K. Poly Degrad Stab 2003, 79, 183.
13. Ursu, F. La résonance paramagnétique électronique. Dunod: Paris, 1968; p 142.
14. Metz, G.; Wu, X.; Smith. S. O. J Magn Reson 1994, A110, 219.
15. Bennett, A. E.; Rienstra, C. M.; Auger, M.; Lakshmi, K. V.; Griffin R. G. J Chem Phys 1995, 103, 6951.
16. Sadki, S.; Schottland, P.; Brodie, N.; Sabouraud, G. Chem Soc Rev 2000, 29, 283.
17. Can, M.; Pekmez, K.; Peknez, N.; Yildiz, A. T. R. Turk J Chem 1998, 22, 47.
18. Kipbooms, R.; Menon, R.; Lee, K. In Handbook of Advanced Electronic and Photonic Materials and Devices: Synthesis, Electrical and Optical Properties of Conjugated Polymers; Nalwa, H. S., Ed.; Vol. 8, Academic Press: New York, 2001; p 12.
19. Fréchette, M.; Belletête, M.; Bergeron, J. Y.; Durocher, G.; Leclerc, M. Synth Met 1997, 84, 223.
20. Ayachi, S.; Saïd, A. H.; Molinié, P.; Alimi, K. Synth Met 2004, 143, 103.
21. The Handbook on Infrared and Raman Characteristic Frequencies of Organic Molecules, Academic Press: New York, 1989.
22. Bongini, A.; Brioni, F.; Panunzio, M. J Chem Soc Perkin Trans 1997, 2, 927.